Electrical Characteristics of Single Layer Graphene Ribbons in a Wide Temperature Range

Rachid FATES [1], Riad REMMOUCHE [1, 2] *, Toufik BENKEDIDAH [1, 3]

[1] *Department of Electronics, MSB Jijel University, B.P. 98, Ouled Aissa, Jijel, 18000 Algeria*
[2] *LEM Laboratory, Jijel University, B.P. 98, Ouled Aissa, Jijel, 18000 Algeria*
[3] *NDT Laboratory, Jijel University, B.P. 98, Ouled Aissa, Jijel, 18000 Algeria*

http://doi.org/10.5755/j02.ms.33700

Received 05 April 2023; accepted 13 June 2023

This paper provides electrical characterization of single layer graphene ribbon devices defined as back-gated graphene transistors. The two-terminal back-gated graphene ribbon devices were fabricated on a conventional Si substrate covered by a 90 nm-thick thermal SiO_2. The chemical vapor deposition process was used for the graphene layer deposition and its quality was checked with optical microscopy, scanning electron microscopy and Raman spectroscopy. For the device fabrication, optical lithography was used for electrode patterns through a mask, and Ti/Au (10 nm/100 nm) metallic contacts were deposited by thermal evaporation. We report low and high field electrical measurements of several devices, under a controlled environment over a wide temperature range, from 77 to 300 K. At 77 K, the drain current decreases, i.e. the resistance of the graphene increases, and the nonlinearity is still present. The maximum influence of the temperature is reached at the charges neutrality point, and we observe that the temperature could influence the position of the charge neutrality point. This indicates that the carriers are thermally activated, which yields a least pronounced current with the increase of the back gate voltage.

Keywords: graphene, nanoribbons, characterization, Raman spectroscopy, temperature.

1. INTRODUCTION

Graphene was isolated and characterized for the first time utilizing the "Scotch Tape" method by Geim and Novoselov in 2004 and since graphene research has accelerated exponentially [1]. This discovery was followed by the study of the electrical properties of this material treated in a large number of academic publications. It consists of a single-atom-thick carbon sheet arranged in a two-dimensional (2D) hexagonal lattice with sp^2 bonded carbon of a length of 1.42 Å. Graphene-based devices offer multiple functions of signal emission, transmission, modulation, and detection, featured with broad band, high speed, compact size, and particularly low loss [2 – 4]. By comparing with the materials currently used such as silicon [5 – 7], graphene possesses unique characteristics in its high electron mobility, large thermal conductivity, strong mechanical properties, and high third-order optical nonlinearities.

For two decades, significant attention has been devoted to graphene by research groups across the world promising potential applications including longer-lasting batteries [8 – 10], more efficient solar cells [11], circuit boards [12] and medicinal technologies such as the detection of diseases [13 – 15].

In the literature, several studies [16 – 21] have reported current-voltage characteristics of graphene devices with different architectures. However, few studies [22] reported the electrical characteristics and temperature dependence of graphene devices. In our previous experiment [23], we carried out a study on graphene ribbons' electrical behavior. We found evident measurements of linear and nonlinear transport mechanisms in large graphene ribbons and in the present investigation, we report the measurements of electrical behaviors at low temperatures in graphene ribbons produced by Chemical vapor deposition (CVD) techniques.

Here we investigate the transport mechanisms in devices biased up to 60 volts. First, we describe the device fabrication process and the presentation of initial characterizations, including scanning electron microscopy (SEM) and the Raman characterizations, that show the studied devices and highlighted the quality of the graphene. Next, we describe both the experimental fabrication process and the electrical measurement setup. Thereafter, we address the characteristics of graphene ribbon devices at high bias for 300 K and 77 K temperatures. Finally, in the results and discussion section, we report the results on the impact of low temperatures on linear and nonlinear electrical behaviors leading to an original conclusion.

2. EXPERIMENT

Two-terminal back gated graphene ribbon devices are fabricated with a lithographic process. First, copper (Cu) foil was used as a substrate for graphene growth. The Cu foil was annealed at 1050 °C in a CVD furnace, and the methane was used as a carbon atoms precursor. Thereafter, to prepare the graphene transfer to a silicon dioxide (SiO_2) on silicon (Si) substrate, the surface of the graphene on Cu was coated with polymethyl methacrylate (PMMA). The Cu foil was etched, resulting in graphene/PMMA films floating on the etchant. Thereby, the graphene layer was transferred onto

* Corresponding author. Tel.: +312-7-75187568.
E-mail: *remmouche@univ-jijel.dz* (R. Remmouche)

heavily p-doped SiO_2 on a Si substrate covered with a 90 nm thick thermal SiO_2 layer. These films were then collected onto a SiO_2/Si substrate, and the PMMA layer was removed with acetone, yielding to graphene/SiO_2/Si structure. Further details concerning the graphene growth parameters, the graphene transfer process and other kinetic and thermodynamic are reported in reference [23]. Then, the quality of graphene is checked with optical microscopy, scanning electron microscopy and Raman spectroscopy, as shown in Fig. 1 and Fig. 2. Finally, for the source/drain pads, optical lithography was used for electrode patterns through a mask, followed by deposition of Ti/Au (10 nm/100 nm) as the metallic contact on the graphene by thermal evaporation.

The graphene ribbons' dimensions are 16 µm wide by 10 µm long. The typical 3D perspective model of the fabricated devices is given in Fig. 1 a. The ribbon between both top metallic contacts is clearly highlighted in the SEM picture as shown in Fig. 1 b. The data were acquired with a micro-Raman spectrometer (LabRAM HR Horiba), a×100 objective using a laser excitation wavelength of 514.5 nm (the excitation energy is 2.41 eV), and a 2400 grooves/mm grating is used.

The electrical characteristics of graphene ribbons at low temperatures were collected in a vacuum using a microprobe station (CPX Cryogenics 6-probe) equipped with a vacuum chamber and a thermal chamber. The temperature-dependent current-voltage measurements were performed in the temperature range of 300 K – 77 K using the thermal chamber. The current-voltage data were collected by an Agilent K4200-SCS analyzer. A graphical summary of the measurement setup is shown in Fig. 2.

3. RESULTS AND DISCUSSION

The Raman spectra, of the localized points in Fig. 1 b, are given in Fig. 1 c. Raman spectroscopy was performed to confirm the formation of graphene and to obtain information about the quality and the number of graphene layers. The intensity ratio I(2D)/I(G) is between 1.9 and 2.2, and the 2D peak is fitted by one single Lorentzian component, these both features indicate that the graphene ribbon is a single layer, which is in line with what is reported in the literature [24, 25].

3.1. Room temperature characteristics

The electrical characteristics of graphene ribbons for various biases were measured at room temperature. We identify two typical output characteristics measurements: the measurements showing a nonlinear (NL) behavior, and the measurements showing a linear (L) behavior. These measurements are presented in Fig. 3. As we observe in Fig. 3 a and Fig. 3 c, the drain to source current (I_{ds}) decreases as the gate voltage increases from 0 V to 50 V. This trend indicates that the single layer ribbon is p-type. Thereby, the comparison between the measurements shown in Fig. 3(a) and 3(c) shows that the current intensity is more important in the linear device, which reveals that the device that exhibits a linear behavior is more doped than the second one that exhibits a nonlinear behavior.

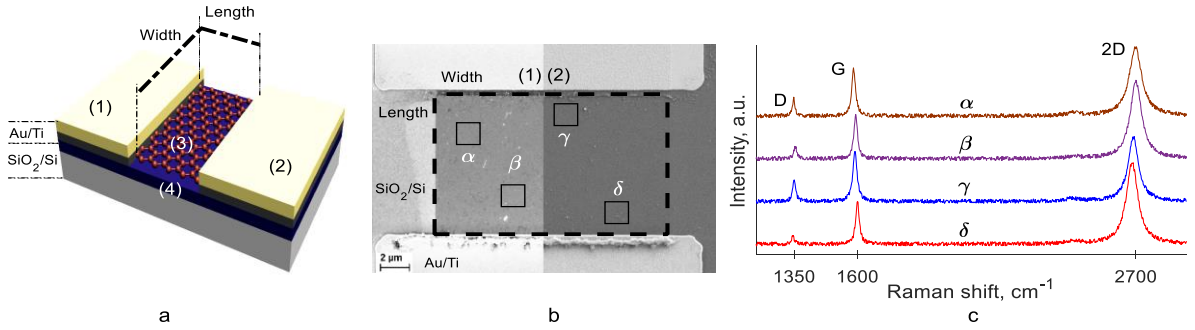

Fig. 1. Description of the fabricated device: a – 3D perspective view of the device structure: (1, 2) Au/Ti metallic contacts, (3) graphene ribbon, (4) Si substrate covered by a 90 nm thick SiO_2 layer; b – SEM image of graphene ribbon device, analyzed with (1) InLens detector and (2) SE2 detector; c – Raman spectra of the localized points in graphene ribbon in panel b showing the main D, G and 2D peaks

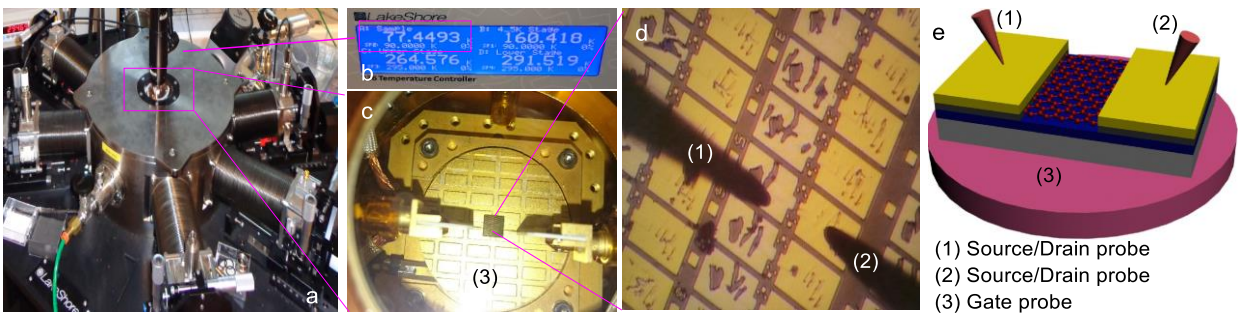

Fig. 2. Thermal measurements: a – CPX Station; b – sample temperature indicator; c – photograph of the thermal chamber indicating the device and the measurement probes; d – optical micrograph of one device during the electric measurement. The source/drain probes are indicated as (1) and (2); e – 3D perspective view of one device showing the position of (1,2) the source/drain probes and (3) the gate probe

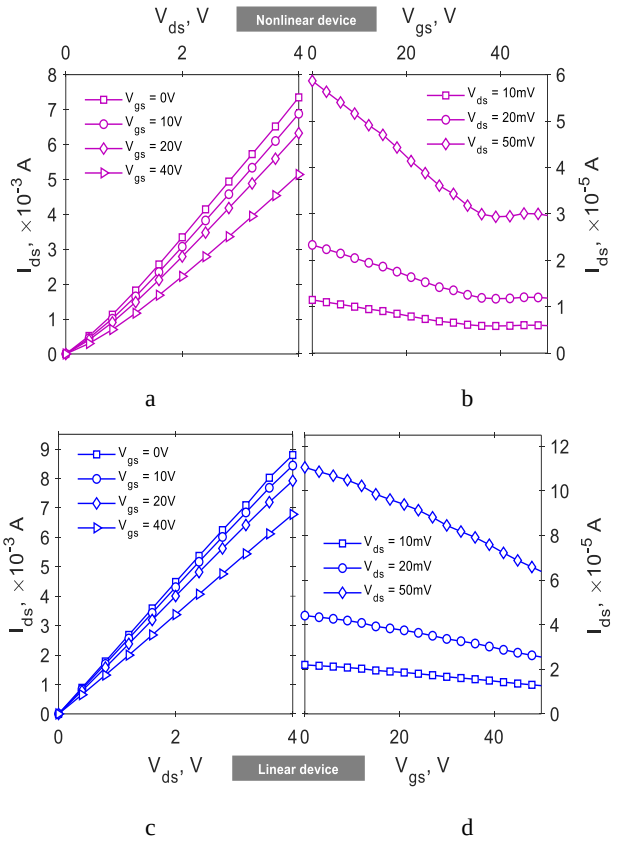

Fig. 3. Measurements extracted on two devices at room temperature: a – output and b – transfer characteristics of the nonlinear behavior on the first device; c – output and d – transfer characteristics of the linear behavior on the second device

These results are in line with the transfer characteristics shown in Fig. 3 b and Fig. 3 d, where, we observe that the Dirac point is located around V_{gs} = 39 V, while, the Dirac point for the nonlinear device is located beyond 60 V. We could not define a precise value of the linear device because the device does not resist to voltage range beyond 60 V, i.e. it is obvious that all the devices electrical characteristics are strongly dependent on the ribbon's biases.

For the nonlinear behavior, the output characteristics exhibit two regimes. The first regime, for low drain voltage, V_{ds} < 1 V, defines an ohmic low voltage regime. The second regime for the higher drain to source voltages, V_{ds} > 1 V, shows an avalanche effect. Graphically, both slopes intersect at a point defining a regime change.

In previous studies, Shin et al. [26] attributed the nonlinearity in single layer graphene devices to the presence of doping sources in graphene such as impurities and active radicals. Nevertheless, Fates et al. [23] report that the linear behavior attests that we can get a linear behavior for high doped graphene. The linear behavior reveals that the Au/Ti/p-type-graphene junction is ohmic. For graphene ribbon-based structures, the local carrier density along the channel plays an important role in the transport properties, indeed, the linear behavior is due to highly doped graphene, while the nonlinear behavior is strongly related to the graphene localized doping.

3.2. Temperature dependence

The temperature dependence of the device electrical output characteristics is presented in Fig. 4 for both nonlinear and linear behaviors. As the temperature decreases, the drain-source current characteristics varies for both behaviors, therefore, the temperature has a relevant influence on the current characteristics of the devices. When gate voltage (V_{gs}) vary from 0 V to 40 V, we observe similar trends of the output characteristics at 300 K as well for nonlinear as for linear behaviors with respect to those observed at room temperature for the same gate voltage. However, at 77 K the current decreases in all configurations. In terms of curves shapes, both nonlinear and linear behaviors were observed at 77 K.

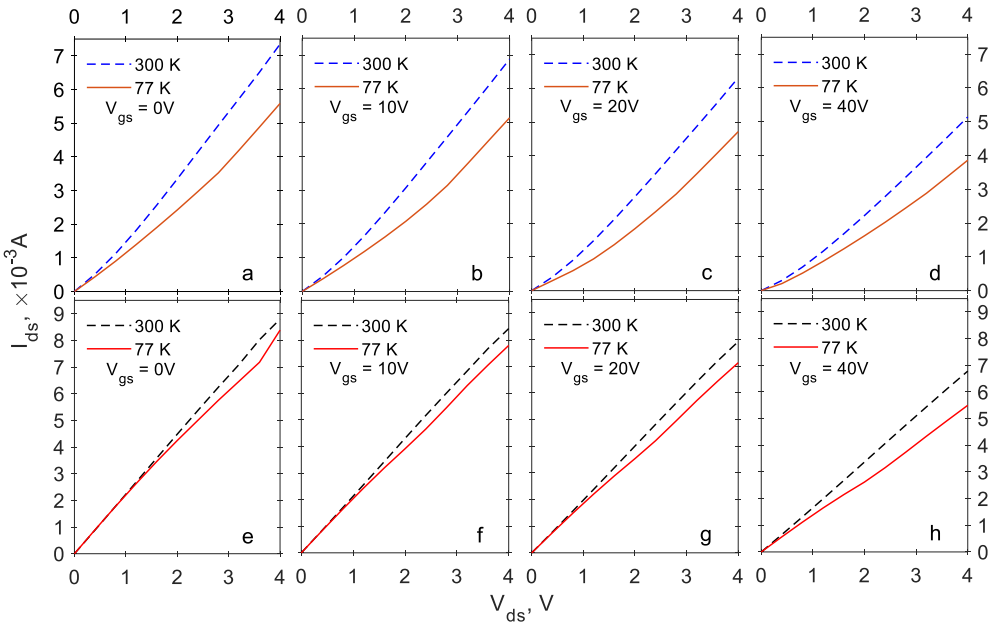

Fig. 4. Comparison of output characteristics measurements for (a – d) nonlinear behavior and (e – h) linear behavior at 300 K and 77 K for gate voltage ranging from 0 V to 40 V

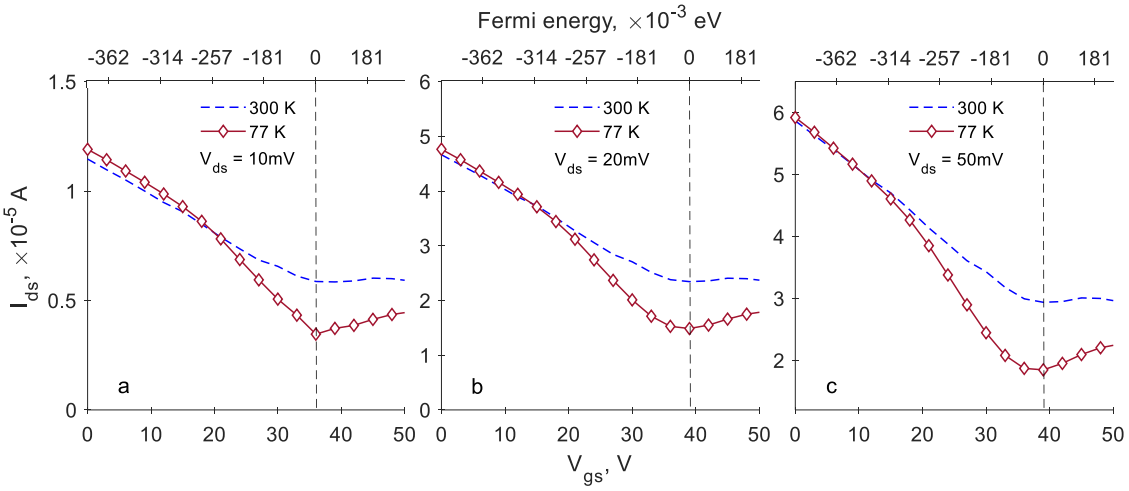

Fig. 5. Measurements of the transfer characteristics of the nonlinear device. The measurements were performed at 300 K and 77 K temperatures

Nevertheless, for the same V_{gs} value, the nonlinear behavior exhibits a more important change in current than the linear behavior. At low temperatures, the doping is less important at 77 K than at room temperature, which is compatible with the presence of nonlinear behavior. Following the results of Fig. 4, both electrical behaviors shapes appear independent of the temperature, this is due to the fact that the graphene ribbons are relatively highly doped which is in agreement with the results of the reference [23]. A previous study [22] reports that, at the cryogenic temperature, the nonlinearity is most pronounced with the increasing of the gate voltage value. In our case, the measurements are made down to 77 K, while the gate voltage increases the nonlinearity is still present, this result means that the nonlinearity is independent of the back gate field effect influence.

As the gate voltage increases, the drain-source current decreases down to the minimum value at the Dirac point, which explains that the graphene ribbon is p-doped. This trend is observed as well at 300 K as at 77 K. The difference in the current transport regime for both temperatures is observed at the voltage V_{gs} = 20 V which corresponds to the Fermi energy E_F = ~257 meV. For V_{gs} < 20 V, as well at 300 K as at 77 K, the curves show that the current has the same evolution, which could be explained by the fact that in this voltage range, the graphene is highly doped. For V_{gs} > 20 V, the impact of the temperature is highlighted. Indeed, the current curves for both temperatures are different and the maximum influence of the temperature is reached at the charges neutrality point. For the n-doping, we observe the same trends with respect to p-doping range. Otherwise, we observe a slight shift of the charges neutrality point at 77 K, from $V_{Dirac} = V_{gs}$ = 37 V for V_{ds} = 10 mV, to $V_{Dirac} = V_{gs}$ = 39 V for V_{ds} = 20 mV and V_{ds} = 50 mV. This is an important result that proves the temperature could influence the position of the charges' neutrality point.

In Fig. 6, the charges neutrality point could not be identified either at 300 K or at 77 K. Moreover, the impact of the temperature is more important when V_{gs} keep rising from V_{gs} > 20 V. Since the charges neutrality point is located beyond 60 V despite the change in temperature, the results of Fig. 6 mean that the graphene ribbon is very highly doped, which will be reflected on the graphene resistance. The ribbons resistance measurements for both nonlinear and linear behaviors are also reported in Fig. 7. In Fig. 7 a, the resistance of the graphene ribbon has a maximum value at the charges neutrality point. When the Fermi level moves from the Dirac point, the resistance increases because there more carriers participate in current transport.

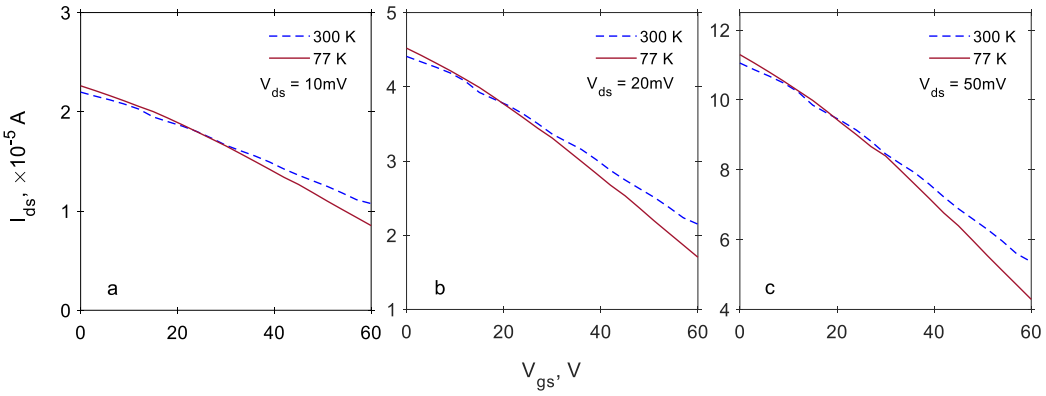

Fig. 6. Measurements of the transfer characteristics of the linear device performed at 300 K and 77 K

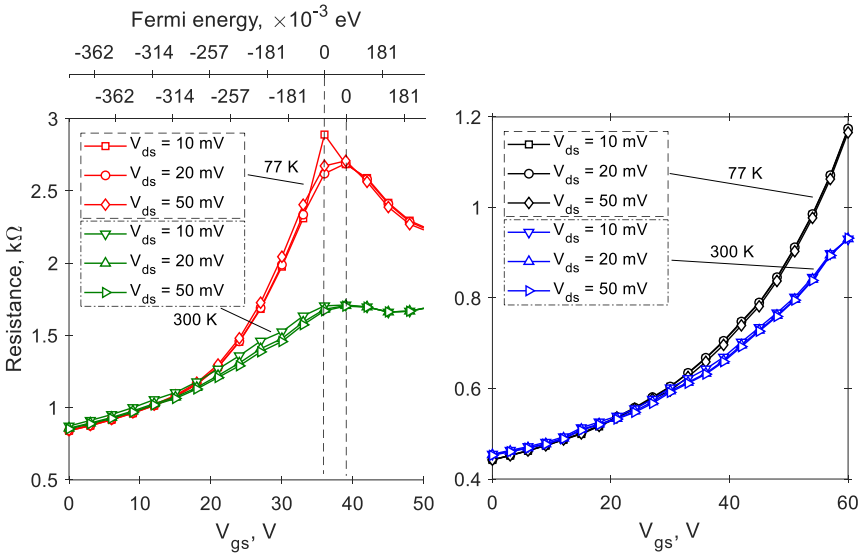

Fig. 7. Resistance measurement comparison: a – for the case of nonlinear behavior device; b – the case of linear behavior device. The measurements were performed at 300 K and 77 K

At 77 K, the resistance of the graphene is more important, i.e. the drain current is less important. This result indicates that the carriers are thermally activated, resulting in the least pronounced current with the increase of the back gate voltage. The shift of the charges neutrality point is clearly visible between V_{ds} = 10 mV and V_{ds} = 20 mV, only at 77 K. In Fig. 7 b, the resistance of linear device increases with the increase of V_{gs} for both 300 K and 77 K temperatures, this result is the consequence of the p-doping of the graphene.

4. CONCLUSIONS

Our study introduces two categories of electrical behavior in back-gated graphene ribbons. The temperature dependence is discussed. The electrical measurements at 300 K and 77 K reveal the presence of nonlinear electrical behavior. This behavior opens the perspective of new electronic behavior in graphene field effect devices. Our results show that the doping is less important at 77 K than at room temperature, which is compatible with the presence of the nonlinear behavior even for temperatures as low as 77 K. At this temperature, the maximum influence of the temperature is reached at the charges neutrality point, and we observe that the temperature could influence the position of the charges neutrality point. The charge transport exhibits a transition between the thermally activated current transport at room temperatures and variable range hopping at lower temperatures. This could be explained by the fact that the thermal charging effects constitute a significant portion of the activation energy.

Acknowledgments

The authors would like to thank Prof. J. P. Raskin and the graphene team of ICTEAM at Université Catholique de Louvain, Louvain – la – Neuve (Belgium) for supporting all the measurements.

REFERENCES

1. **Novoselov, K.S., Geim, A.K., Morozov, S.V., Jiang, D., Zhang, Y., Dubonos, S.V., Grigorieva, I.V., Firsov, A.A.** Electric Field Effect in Atomically Thin Carbon Films *Science* 306 (5696) 2004: pp. 666 – 669. https://doi.org/10.1126/science.1102896
2. **Vicarelli, L., Vitiello, M.S., Coquillat, D., Lombardo, A., Ferrari, A.C., Kap, W., Polini, M., Pellegrini, V., Tredicucci, A.** Graphene Field-Effect Transistors as Room-Temperature Terahertz Detectors *Nature Materials* 11 (10) 2012: pp. 865 – 871. https://doi.org/10.1038/nmat3417
3. **Wang, R., Ren, X.G., Yan, Z., Jiang, L.J., Sha, W.E.I., Shan, G.C.** Graphene Based Functional Devices: A Short Review *Frontiers of Physics* 14 (1) 2019: pp. 1 – 20. https://doi.org/10.1007/s11467-018-0859-y
4. **Yang, J., Hu, P.A., Yu, G.** Perspective of Graphene-Based Electronic Devices: Graphene Synthesis and Diverse Applications *APL Materials* 7 (020901) 2019: pp. 1 – 7. https://doi.org/10.1063/1.5054823
5. **Lin, C.Y., Ulaganathan, R.K., Sankar, R., Murugesan, R.C., Subramanian, A., Rozhine, A., Firdoz, S.** Silicon-based Two-dimensional Chalcogenide of P-Type Semiconducting Silicon Telluride Nanosheets for Ultrahigh Sensitive Photodetector Applications *Journal of Materials Chemistry C* 9 (32) 2021: pp. 10478 – 10486. https://doi.org/10.1039/D1TC02129J
6. **Remmouche, R., Fates, R., Bouridah, H.** Analytical Threshold Voltage Model Considering Quantum Size Effects for Nanocrystalline Silicon *Acta Physica Polonica A* 132 (4) 2017: pp. 1230 – 1233. https://doi.org/10.12693/APhysPolA.132.1230
7. **Fates, R., Bouridah, H., Remmouche, R.** Theoretical Determination of the Impact of Channel Morphology and Quantum Size Effects on the Surface Potential of Nanocrystalline Silicon Thin Film Transistors *Material Science in Semiconductor Processing* 24 (8) 2014: pp. 278 – 281. https://doi.org/10.1016/j.mssp.2014.03.025

8. **Randviir, E.P., Brownson, D.A.C., Banks, C.E.** A Decade of Graphene Research: Production, Applications and Outlook *Materials Today* 17 (9) 2014: pp. 426 – 432. https://doi.org/10.1016/j.mattod.2014.06.001
9. **Latha, M., Vatsala Rani, J.** WS2/Graphene Composite as Cathode for Rechargeable Aluminum-Dual Ion Battery *Journal of Electrochemical Society* 167 (7) 2020: pp. 1 – 8. https://doi.org/10.1149/2.0012007JES
10. **Pender, J.P., Xiao, H., Dong Cavallaro, K.A., Weeks, J.A., Heller, A., Ellison, C.J., Mullins, C.B.** Compact Lithium-Ion Battery Electrodes with Lightweight Reduced Graphene Oxide/Poly(Acrylic Acid) Current Collectors *ACS Applied Energy Materials* 2 (1) 2019: pp. 905 – 912. https://doi.org/10.1021/acsaem.8b02007
11. **Peng, J.D., Wu, Y.T., Yeh, M.H., Kuo Vittal, Y.R., Ho, K.C.** Transparent Cobalt Selenide/Graphene Counter Electrode for Efficient Dye-Sensitized Solar Cells with $Co^{2+/3+}$-Based Redox Couple *ACS Applied Materials and Interfaces* 12 (40) 2020: pp. 44597 – 44607. https://doi.org/10.1021/acsami.0c08220
12. **Hyun, W.J., Park, O.O., Chin, B.D.** Foldable Graphene Electronic Circuits Based on Paper Substrates *Advanced Materials* 25 (34) 2013: pp. 4729 – 4734. https://doi.org/10.1002/adma.201302063
13. **Cellot, G., Biagioni, A.F., Ballerini, L.** Nanomedicine and Graphene-Based Materials: Advanced Technologies for Potential Treatments of Diseases in the Developing Nervous System *Pediatric Research* 92 (6) 2021: pp. 71 – 79. https://doi.org/10.1038/s41390-021-01681-6
14. **Seifi, T., Kamali, A.R.** Antiviral Performance of Graphene-Based Materials with Emphasis on COVID-19: A Review *Medicine in Drug Discovery* 11 2021: pp. 1 – 9. https://doi.org/10.1016/j.medidd.2021.100099
15. **Xie, J., Chen, Q., Shen, H., Li, G.** Review – Wearable Graphene Devices for Sensing *Journal of Electrochemical Society* 167 (3) 2020: pp. 1 – 10. https://doi.org/10.1149/1945-7111/ab67a4
16. **Ashery, A., Farag, A.A.M., Moussa, M.A., Turky, G.M.** Electrical Performance of Nanocrystalline Graphene Oxide/Sio_2-Based Hybrid Heterojunction Device *Material Science in Semiconductor Processing* 121 (1) 2021: pp. 1 – 10. https://doi.org/10.1016/j.mssp.2020.105415
17. **Rui, C., Shao Liu, C.J., Chen, A., Zhu, K., Shao, Q.** Transport Properties of B/P Doped Graphene Nanoribbon Field-Effect Transistor *Material Science in Semiconductor Processing* 130 (8) 2021: pp. 1 – 7. https://doi.org/10.1016/j.mssp.2021.105826
18. **Ryzhii, V., Ryzhii, M., Satou, A., Otsuji, T.** Current-voltage Characteristics of a Graphene-Nanoribbon Field-Effect Transistor *Journal of Applied Physics* 103 (9) 2008: pp. 1 – 8. https://doi.org/10.1063/1.2917284
19. **Schwierz, F.** Graphene Transistors *Nature Nanotechnology* 5 (7) 2010: pp. 487 – 498. https://doi.org/10.1038/nnano.2010.89
20. **Sharma, B.K., Ahn, J.H.** Graphene Based Field Effect Transistors: Efforts Made Towards Flexible Electronics *Solid-State Electronics* 89 (11) 2013: pp. 177 – 188. https://doi.org/10.1016/j.sse.2013.08.007
21. **Song, S.M., Bong, J.H., Hwang, W.S., Cho, B.J.** Improved Drain Current Saturation and Voltage Gain in Graphene–on–Silicon Field Effect Transistors *Scientific Reports* 6 (5) 2016: pp. 1 – 7. https://doi.org/10.1038/srep25392
22. **Wang, P.H., Shih, F.Y., Chen, S.Y., Hernandez, A.B., Ho, P.H., Chang, L.Y., Chen, C.H., Chiu, H.C., Chen, C.W., Wang, W.H.** Demonstration of Distinct Semiconducting Transport Characteristics of Monolayer Graphene Functionalized via Plasma Activation of Substrate Surfaces *Carbon* 93 (11) 2015: pp. 353 – 360. https://doi.org/10.1016/j.carbon.2015.05.060
23. **Fates, R., Raskin, J.P.** Linear and Non-Linear Electrical Behaviors in Graphene Ribbon Based Devices *Journal of Science: Advanced Materials and Devices* 3 (3) 2018: pp. 366 – 370. https://doi.org/10.1016/j.jsamd.2018.06.001
24. **Fates, R., Bouridah, H., Raskin, J.P.** Probing Carrier Concentration in Gated Single, Bi- and Tri-layer CVD Graphene Using Raman Spectroscopy *Carbon* 149 (8) 2019: pp. 390 – 399. https://doi.org/10.1016/j.carbon.2019.04.078
25. **Fates, R., Remmouche, R., Benkedidah, T., Raskin, J.P.** Evolution of the Raman Spectra Features of Defective Monolayer Graphene in Back-Gate Configuration: Experimental Study *Diamond and Related Materials* 136 (6) 2023: pp. 1 – 7. https://doi.org/10.1016/j.diamond.2023.109919
26. **Shin, Y.J., Gopinadhan, K., Narayanapillai, K., Kalitsov, A., Bhatia, C.S., Yang, H.** Stochastic Nonlinear Electrical Characteristics of Graphene *Applied Physics Letters* 102 (3) 2013: pp. 1 – 5. https://doi.org/10.1063/1.4788737